arXiv:2007.00838v2 [quant-ph] 24 Dec 2020

Quantum optimal control of multi-level dissipative quantum systems with Reinforcement Learning

Zheng An,[1,2] Hai-Jing Song,[1,2] Qi-Kai He,[3] and D. L. Zhou[1,2,4,5,*]

[1] *Institute of Physics, Beijing National Laboratory for Condensed Matter Physics, Chinese Academy of Sciences, Beijing 100190, China*
[2] *School of Physical Sciences, University of Chinese Academy of Sciences, Beijing 100049, China*
[3] *HangZhou Tuya Information Technology Co., Ltd, Hangzhou, Zhejiang 310000, China*
[4] *Collaborative Innovation Center of Quantum Matter, Beijing 100190, China*
[5] *Songshan Lake Materials Laboratory, Dongguan, Guangdong 523808, China*

(Dated: January 22, 2022)

Manipulate and control of the complex quantum system with high precision are essential for achieving universal fault tolerant quantum computing. For a physical system with restricted control resources, it is a challenge to control the dynamics of the target system efficiently and precisely under disturbances. Here we propose a multi-level dissipative quantum control framework and show that deep reinforcement learning provides an efficient way to identify the optimal strategies with restricted control parameters of the complex quantum system. This framework can be generalized to be applied to other quantum control models. Compared with the traditional optimal control method, this deep reinforcement learning algorithm can realize efficient and precise control for multi-level quantum systems with different types of disturbances.

I. INTRODUCTION

Precise and complete control of complex quantum systems is the core to achieve quantum computation and quantum information processing. The quantum control (QC) theory provides a powerful tool to achieve high precision control of quantum dynamics. A QC problem can be phrased as finding strategies of inducing complete transfer of population from an arbitrary initial quantum state to the desired target state. An optimal strategy to get a selected state of a finite energy level quantum system is of primary importance for the control of quantum dynamics. The theory for design such an optimal strategy has been studied widely, such as Lyapunov quantum control [1, 2], geometric control theory [3], and Pontryagin maximum principle [4]. Also, robust and optimal strategies of QC is essential for many areas of physical systems from nitrogen-vacancy center experiments [5], optical systems[6] to superconducting qubits [7]. However, it is hard to get a convincing result with traditional control theory if there have some restricted conditions in the control system. To manipulate more complicated systems, there have been developed sever algorithms in numerical, like GRAPE [8, 9] and CRAB [10, 11]. Further, the disturbance of quantum dynamics is the main obstacle in implementing scalable quantum computing [12]. To deal with the spin or qubit decoherence, various strategies have been developed, including quantum error correction [13–16], dynamical decoupling (DD) [17–19], and optimized control in protecting quantum coherence [20–22]. One way to achieve the optimal control is to use an arbitrarily slow change of the dynamical parameters and the adiabatic theorem [23]. However, for a multi-level system, these require several resources that also increase exponentially with the size of the system. On the other hand, when applied to a typical realistic condition of an open quantum system is considered, there are few analytical or ansatz solutions available. To simplify those constraints, here we introduce a switch on-off control problem with dissipative dynamics in this paper. In particular, we discuss the dynamics that are affected by dephasing and energy decay. These two effects exist, to different degrees, in any practical attempt to implement quantum control tasks in real physical systems [24–27]. Those disturbances effects emerge from the interaction of the system with the surrounding environment [28].

Quantum control theory has been recently applied with success to the optimization of the dynamics of simple systems [29–32] and quantum many body systems [10, 11, 33, 34]. With the progress of quantum control techniques and computer science, the numerical algorithm gives us a robust and efficient way to implement high-fidelity quantum control. Among various control algorithms, reinforcement learning (RL) has been attracting much focus. Reinforcement learning has demonstrated remarkable abilities in board games [35–37] and video games [38–40]. Recently it has also been widely applied to a wide array of physics problems, such as quantum state preparation [33, 41], quantum gate control [42, 43], quantum error correction [44], and quantum metrology [45]. Those successes naturally raise the question of how much quantum control might benefit from the application of reinforcement learning.

In this paper, we study a general quantum control model of a finite-level system under disturbances. To explore the optimal strategy of the control problem in this scenario, we use the distributed proximal policy optimization (DPPO) algorithm [46, 47] to study this problem in this paper. The proximal policy optimization (PPO) algorithm has been successfully used in

* zhoudl72@iphy.ac.cn

robotics [48] and aircraft control [49]. Recently, it has been applied in QC problems [50, 51].

The rest of this paper is structured as follows. In Sec. II, we briefly introduce the basic description of our quantum control model. In Sec. III, we present the Actor-Critic model of Reinforcement learning and DPPO algorithm used in our paper. In Sec. IV, we present the methodology of our method, the architecture of the neural network for our agent, the interactive interface as well as numerical results of tested examples. Finally, in Sec. V, we draw our conclusions.

II. MODEL

We study a quantum system with a finite number of distinct energy levels driven by a time-dependent external field whose Hamiltonian reads:

$$H = H_0 + V \tag{1}$$

with

$$H_0 = \sum_{i=1}^{n} E_i |i\rangle\langle i|, \tag{2}$$

$$V(t) = \sum_{i=1}^{n-1} \gamma(t) \left(|i\rangle\langle i+1| + |i\rangle\langle i+1| \right), \tag{3}$$

where H_0 is called the drift Hamiltonian and $V(t)$ is called the control Hamiltonian in quantum control theory. The state $|i\rangle$ is the i-th eigenstate of H_0 with eigenenergy E_i, n is the number of the energy levels, and the time-dependent real parameter $\gamma(t)$ is the coupling strength between $|i\rangle$ and $|i+1\rangle$ for $1 \leq i \leq n-1$. Without losing of generality, we assume that $E_1 \leq E_2 \leq \cdots \leq E_n$. In particular, we assume H_0 is regular, where the energy levels $E_i = i$ $(i = 1, \ldots, n)$. However, a different distribution of eigenenergies may affect the performance of control algorithms. So we presented the effect of the different distribution of eigenenergies on two examples in Appendix D.

When our system weakly interacts with its environment, its dynamics is described by the master equation of the Lindblad type:

$$\dot{\rho} = -\frac{i}{\hbar}[H, \rho] + \sum_k \Gamma_{k,n} \left(A_{k,n} \rho A_{k,n}^\dagger - \frac{1}{2} \left\{ A_{k,n}^\dagger A_{k,n}, \rho \right\} \right), \tag{4}$$

where $A_{k,n}$ is the Lindblad operator associated with some dissipative process with a decay rate $\Gamma_{k,n}$ for each k, and the subscript n labels the type of dissipative process. $\{A, B\} = AB + BA$ denotes the anticommutator. Here we consider two typical dissipative processes. One is the dephasing process, whose Lindblad operator $A_{k,d} = |k\rangle\langle k|$ with an identical dephasing rate $\Gamma_{k,d} = \Gamma_d$ for $1 \leq k \leq n$. The other is the energy decay process, whose Lindblad operator $A_{k,l} = |1\rangle\langle k|$ with an identical energy decay rate $\Gamma_{k,l} = \Gamma_l$ for $2 \leq k \leq n$.

Our central task can be stated as follows. Initially, our system is prepared in the ground state $|1\rangle$ of H_0. By controlling the time dependence of the parameter $\gamma(t)$, we aim to maximize the probability for our system to be in the highest excited state n of H_0 at a fixed time T.

For simplicity, we adopt the bang-bang control protocol. We divide the total control time T into N periods with the same duration $\delta t = T/N$. In the i-th period with $(i-1)\delta t \leq t \leq i\delta t$ $(1 \leq i \leq N)$, the coupling is either switched on or switched off, i.e., $\gamma(t) = a_i \gamma$ with $a_i \in \{0, 1\}$. Then a control strategy is specified by a series of binary numbers $\{a_1, a_2, \cdots, a_N\}$. We aim to find out an optimal strategy to maximize the fidelity

$$\mathcal{F}\left(\rho(T), |n\rangle\langle n|\right) = \langle n|\rho(T)|n\rangle. \tag{5}$$

It is worthy to point out that, since the size of the set of the strategy space is 2^N, it is impossible to get the optimal strategy by exhaustively searching in the strategy space for a large N.

Note that we focus on a regime where γ is much smaller than the energy gap $E_n - E_1$, which implies that the probability of arriving at the state $|n\rangle$ at any time is very small with the coupling always on. However, the optimal strategy to improve the probability of arriving at the highest energy eigenstate of H_0 with switching on/off the coupling V can be understood as follows. First, we switch on the coupling V for a short period from a lower energy eigenstate to a higher energy eigenstate, then we switch off the coupling V to avoid the effect of $|i\rangle\langle i+1|$. Further, when the coupling V is switched off, the free Hamiltonian H_0 changes the state of the system while keeping the energy invariant. Thus the energy of the system can be increased by suitable arranges of switching on/off the coupling.

In fact, we will study the cases where the dimension of the Hilbert space is 4, 6, 8 and 10 while we do not increase the number of the control parameters, which brings a great challenge to get an optimal strategy to arrive at the highest eigenenergy state by a sequence of jumps $|1\rangle \leftrightarrow |2\rangle \leftrightarrow \cdots \leftrightarrow |n\rangle$.

III. REINFORCEMENT LEARNING: ACTOR CRITIC MODEL

To find out the optimal strategy in our multi-level quantum control problem, we will adopt a modern reinforcement learning method called the actor-critic model. In this section, we will give a short review of the actor critic reinforcement learning model.

In the traditional reinforcement learning, there are two different types of methods to implement artificial intelligence. One is the value-based methods (such as the Q-learning [52]), where the agent learns the value function that maps each state-action pair to a value. According to the value function, the agent will take the action with the largest return value for each state. It works well

when the set of actions is finite. The other is the policy-based methods (such as policy gradients [53]), where we directly optimize the policy without using a value function. It is efficient when the action space is continuous or stochastic.

The reinforcement learning process is a finite Markov decision process [53]. As shown in Fig. 1, a state S_t at time t is transmitted into a new state S_{t+1} together with giving a scalar reward R_{t+1} at time $t+1$ by the action A_t with the transmission probability $p(S_{t+1}, R_{t+1}|S_t, A_t)$.

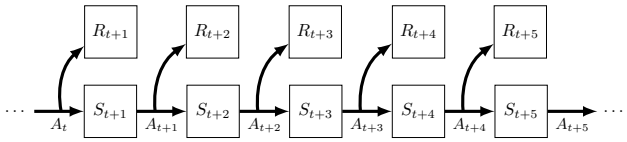


FIG. 1. A schematic diagram of Markov decision process.

For a finite Markov decision process, the sets of the states, the actions and the rewards are finite. In the value based methods, the goal is to maximize the total discounted return at time t

$$G_t = \sum_{k=0}^{\infty} \Gamma^k R_{t+k+1}, \tag{6}$$

where Γ is the discount rate and $0 \leq \Gamma \leq 1$. The policy π is defined by the conditional probability $\pi(a|s)$ of selecting an action a for each state s. To estimate how good a policy π is, two value functions are introduced:

$$q_\pi(s,a) \doteq \mathbb{E}_\pi \left[G_t | S_t = s, A_t = a\right], \tag{7}$$
$$v_\pi(s) \doteq \mathbb{E}_\pi \left[G_t | S_t = s\right], \tag{8}$$

where $q_\pi(s,a)$ is called the state-action value function, $v_\pi(s)$ is called the state value function; E_π denotes the probability expectation for all the actions in the process taken following the policy π. Note that we have the following relations:

$$q_\pi(s,a) = \sum_R Rp(R|s,a) + \Gamma \sum_{s'} v_\pi(s') p(s'|s,a), \tag{9}$$
$$v_\pi(s) = \sum_{R,a} Rp(R|s,a)\pi(a|s) + \Gamma \sum_{s',a} v_\pi(s') p(s'|s,a)\pi(a|s). \tag{10}$$

In addition, the advantage function is defined as $A_\pi(s,a) = q_\pi(s,a) - v_\pi(s)$, which measures the advantage of an action a with respect to the state s under the policy π.

In the policy gradient scheme, the objective is to maximize the cumulant reward under a parameterized policy π_θ:

$$J(\pi_\theta) = \mathbb{E}_{\pi_\theta}\left[\sum_{t=0}^{\infty} \Gamma^t R(s_t)\right]. \tag{11}$$

The model-free policy gradient of the cumulant reward is given by [54]

$$\nabla_\theta J(\pi_\theta) \propto \sum_s \mu(s) \sum_a A_{\pi_\theta}(s,a) \nabla_\theta \pi_\theta(a|s), \tag{12}$$

where $\mu(s)$ is the probability of appearing state s in the Markov process under the policy π. The above gradient can be estimated by the score function estimator [55].

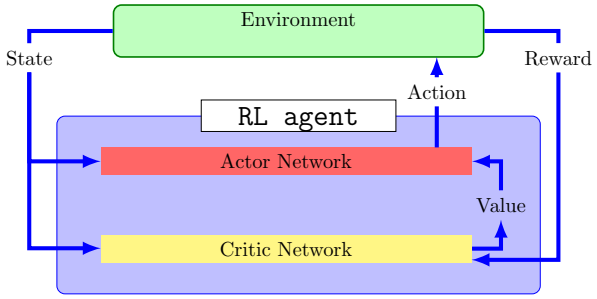


FIG. 2. A schematic diagram of actor-critic model: at each time step of training, the Actor network of the agent proposes a control action of A_t, the environment takes the proposed action and evaluates quantum state for time duration δt to obtain the reward, both of which are fed into the RL agent. The Critic network of the agent receive the reward and estimate the action's value based on the state.

In this paper, we use a hybrid type of reinforcement learning method, called the actor-critic, whose protocol is shown in Fig. 2. The agent has two parts: a critic that measures how good the action taken is and an actor that controls how our agent behaves. The actor builds a network to evaluate the policy π_θ, and takes an action for the current state of the environment following the policy π_θ. The critic builds a network to evaluate the state value function $v_\phi(s)$, which is used to approximate $A_{\pi_\theta}(s,a)$ in Eq. (12). The critic improves the value network according to the reward from the environment, and the actor improves the policy network according to a modified version of Eq. (12):

$$\nabla_\theta J(\pi_\theta) \propto \sum_s \mu(s) \sum_a A_\phi(s,a) \nabla_\theta \pi_\theta(a|s). \tag{13}$$

In the actor-critic model, we get the advantage by building a network, which is more efficient than by directly simulating following the policy π_θ. Besides, it improves the convergence significantly to use the advantage function to replace the state-action value function in evaluating the policy gradient [56].

In this work, we use the distributed proximal policy optimization algorithm (DPPO) [47] to learn an optimal policy under the policy gradient framework. The loss function of DPPO reads

$$L(\theta,\phi)=\hat{\mathbb{E}}_{\pi_{\theta_{\rm old}}}\left[\min\left(r_{\theta_{\rm old}}(a|s_0,\theta)A_\phi(s_0,a),\mathrm{clip}\left(r_{\theta_{\rm old}}(a|s_0,\theta),1-\epsilon,1+\epsilon\right)A_\phi(s_0,a)\right)\right], \tag{14}$$

where ϵ is a hyper-parameter ($\epsilon=0.2$ in this paper). The expectation $\hat{\mathbb{E}}_{\pi_{\theta_{\rm old}}}$ indicates the empirical average over a finite batch of samples under the policy $\pi_{\theta_{\rm old}}$. The term $r_{\theta_{\rm odd}}(a|s,\theta)$ is defined as the ratio of likelihoods

$$r_{\theta_{\rm old}}(a|s,\theta)=\frac{\pi_\theta(a|s)}{\pi_{\theta_{old}}(a|s)}. \tag{15}$$

The clip function for $c\le d$ is defined as

$$\mathrm{clip}(f(x),c,d)=\begin{cases}d, & \text{if } f(x)>d,\\ f(x), & \text{if } c\le f(x)\le d,\\ c, & \text{if } f(x)<c.\end{cases} \tag{16}$$

The clip function for $r_{\theta_{\rm old}}(a|s,\theta)$ penalizes large changes between nearest updates, which corresponds to the trust region of the first order policy gradient. Based on the first-order trust region search gradient descent, DPPO has a robust learning process and can handle both discrete and continuous action spaces. A detailed description of the DPPO can be found in the Appendix C.

IV. QUANTUM STATE CONTROL WITH ACTOR-CRITIC LEARNING

A. Agent-environment interface

To implement the RL agent for our problem, we propose an interactive interface between the RL agent and the physical environment (Fig. 2) adapted to OpenAI Gym [57]. We have used Tensorflow [58] and Baselines [59] to implement the learning algorithms with QuTip [60, 61] simulating the dynamics of our control problem. The architecture of deep neural network in our RL agent is shown in Fig. 3. In our quantum control problem, the state at time t in the reinforcement learning is the state $\rho(t)$, which is expressed by its components:

$$\begin{aligned}s_t=\{&\Re(\rho_{11}(t)),\Im(\rho_{11}(t)),\\ &\Re(\rho_{12}(t)),\Im(\rho_{12}(t)),\dots\\ &\Re(\rho_{nn}(t)),\Im(\rho_{nn}(t))\},\end{aligned} \tag{17}$$

where $\Re(\rho_{ij}(t))$ and $\Im(\rho_{ij}(t))$ are the real and the imaginary part of the component $\rho_{ij}(t)$ respectively. Our action space is formed by a switchable control field $a_t\in\{0,1\}$, which steers our quantum state $\rho(t)$ to $\rho(t+\delta t)$ according to Eq. (4). After evaluating the new state $\rho(t+\delta t)$ the agent obtains the single step reward

$$R_{t+1}=\mathcal{F}(\rho(t+\delta t),|n\rangle\langle n|)-\mathcal{F}(\rho(t),|n\rangle\langle n|), \tag{18}$$

where $\mathcal{F}$ is the fidelity defined by Eq. (5).

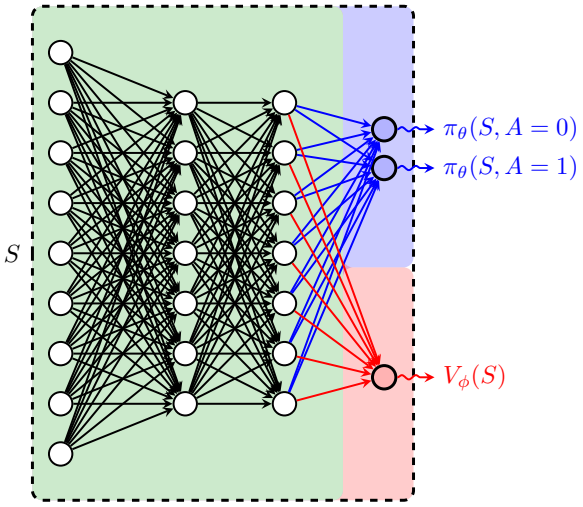


FIG. 3. The architecture of the actor-critic neural network for the agent. The actor and the critic share the same architecture of hidden layers (green). The actor network has an action head (blue) to output the possible policy. The critic network has a value head (red) to output the value of the given state.

B. Numerical results

We now apply the actor-critic RL approach to our quantum state control problem with different settings, illustrating the flexibility and efficiency of our RL agent. Here the different settings include different numbers of energy level for our system, and different types of environments affecting our system. We will give the numerical results of the best fidelity $\mathcal{F}$ in our quantum state control problem from the deep reinforcement learning. To show the effectiveness of our deep RL method, we also calculate the fidelity with the greedy method and gradient ascent pulse engineering (GRAPE) algorithm. The greedy algorithm are used for finding successful policies by performing local searches. The GRAPE method looks at the direct gradient of the fidelity function. In particular, to get better results, the GRAPE algorithm allows for the coupling strength $\gamma(t)$ to take any value in the interval $[0,\gamma]$. We then present our analysis of the performance of our deep RL algorithm against the two algorithms. Details of the greedy algorithm can be found in the appendixes.

1. *Quantum state control without environments*

In this subsection, we consider our quantum state control problem with a quantum system with negligible en-

vironments. In other words, we assume that all the coefficients $\Gamma_{k,n} = 0$.

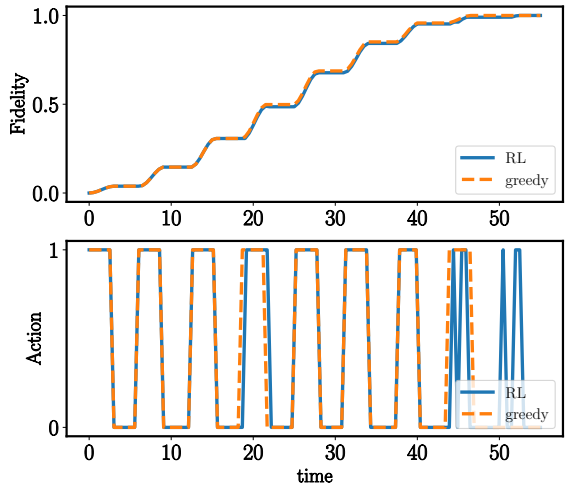


FIG. 4. The best fidelities (up) and strategy (down) of preparing an excited state for the two-level control model with $\gamma = 0.1$. The markers correspond to the algorithms RL (blue line) and greedy (orange line). The time step $N = 110$.

In Fig. 4 we show the results of the optimal fidelity and the corresponding strategy on our quantum state control problem with parameters $\{n = 2, \gamma = 0.1, T = 55, N = 110\}$ in Fig. 4. With 1500 episodes, our RL agent gets the optimal fidelity $\mathcal{F}_{RL}(T) \approx 0.999998$, which is a little larger than the fidelity $\mathcal{F}_{Greedy}(T) \approx 0.999815$ from the direct greedy algorithm. While the difference of the fidelities between those two methods is very small, the strategy in Fig. 4 is different for about $T > 45$, which shows that our RL agent has learned a globally optimized protocol in this task. Notice that for all control tasks discussed in our manuscript, the time scale δt is always 0.5. A detailed optimal strategy of greedy method can be found in the Appendix B.

We further apply our RL agent to the quantum state control problem in the multi-level Hilbert space. We give the optimal fidelities in the cases with the dimension of Hilbert space equal to 4, 6, 8, and 10 by the RL algorithm (red dashed line), the greedy algorithm (blue solid line) and GRAPE (violet dot dashed line), which are shown in Fig. 5(A)-(D). We find that the greedy algorithm becomes less effective with the increase of the dimension of Hilbert space, but the RL algorithm and GRAPE performs well in all cases. For example, when the dimension of Hilbert space varies from 4 to 10, the optimal fidelity from the greedy algorithm varies from about 0.954 to about 0.411, but the fidelity from the RL algorithm varies from about 0.993 to 0.954. While GRAPE has the best performance out of the three methods, the algorithm requires the fidelity gradients at all time.

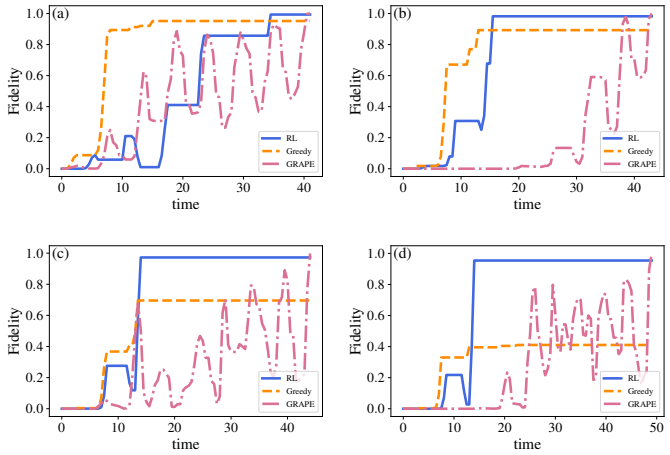


FIG. 5. Results from from the three algorithms for different level control model. The horizontal and vertical axes of each subfigure denote evolution time t and fidelity $\mathcal{F}$. (A),(B),(C),(D): The fidelities for three different methods with 4,6,8,10 level control model. The corresponding coupling strengths with the different models are $\gamma = 0.8, 1.1, 1.4, 1.9$. The time steps with different control tasks are $N = 82, 86, 88, 98$.

2. *Quantum state control with environments*

We now turn our attention to the behavior of our learning strategy when applied to a non-ideal scenario in which typical realistic conditions are considered. In particular, we discuss the results produced by RL agent when the system is affected by dephasing and energy decay.

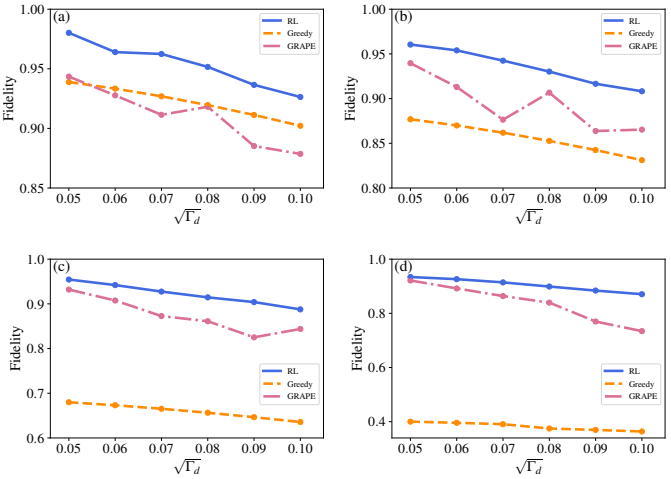


FIG. 6. Results from from the three algorithms for different level control model under dephasing dynamics. The horizontal and vertical axes of each subfigure denote dephasing rate $\sqrt{\Gamma_d}$ and fidelity $\mathcal{F}$. (A),(B),(C),(D): Best fidelity for three different methods of 4,6,8,10 level control model. Note that the Hamiltonian is the same as Fig. 5 showed.

In Fig. 6 we present our numerical results on the control problem under dephasing dynamics. Fig. 6(A)-(D) show the results for dephasing rate $\sqrt{\Gamma_d} = \{0.05, 0.06, 0.07, 0.08, 0.09, 0.1\}$. In both cases, our best results from the RL agent outperform the greedy algorithm and even GRAPE. Also, with the energy level number getting higher, the differences of fidelities between the three methods get larger.

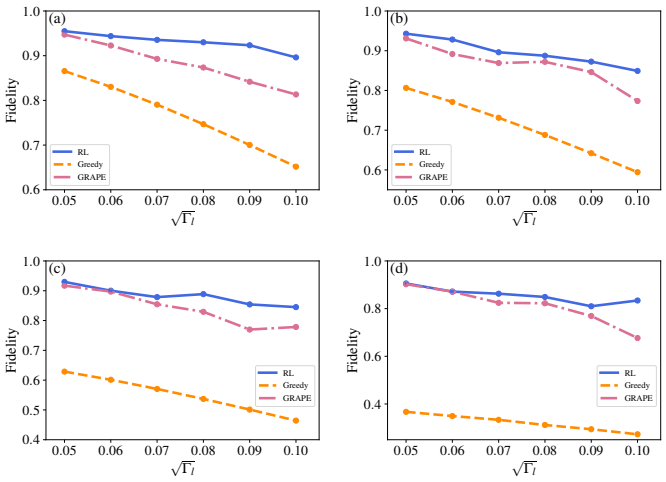


FIG. 7. Results from from the three algorithms for different level control model under energy decay dynamics. The horizontal and vertical axes of each subfigure denote energy decay rate $\sqrt{\Gamma_l}$ and fidelity $\mathcal{F}$. (A),(B),(C),(D): Best fidelity for three different methods of 4,6,8,10 level control model. Note that the Hamiltonian is the same as Fig. 5 showed.

Fig.7 shows the superior performance of the RL agent versus the greedy and GRAPE during the time evolution under the disturbance of energy decay. Similar to the dephasing cases, the RL agent has successfully conquered the control problem under energy decay dynamics. While for the greedy algorithm, it is impossible to get a convincing result with a large energy decay rate in high dimensional control problems. In this scenario, we find that the RL agent successfully learns to adapt to overcome disturbance of energy decay in multi-level control problems.

To further understand the results shown in Fig. 6 and 7, we take examples from $\sqrt{\Gamma_d}, \sqrt{\Gamma_l} = 0.1$ and plot the corresponding trajectories of the fidelity in Fig. 8 and 9. We realized that the RL agent yields different policies according to the types of environments: one only has to learn how to quickly control the state to the target and decide whether to place the control sequence at the beginning or the end of the control. As showed in Fig. 8, the best strategy is to fast drive the initial state to the final state at the start of the control, since the environment cannot change the energy of the system. While in Fig. 8, the strategy becomes opposed as previously shown, the agent learns to avoid a complex control strategy to maintain the target state but to get at the end of

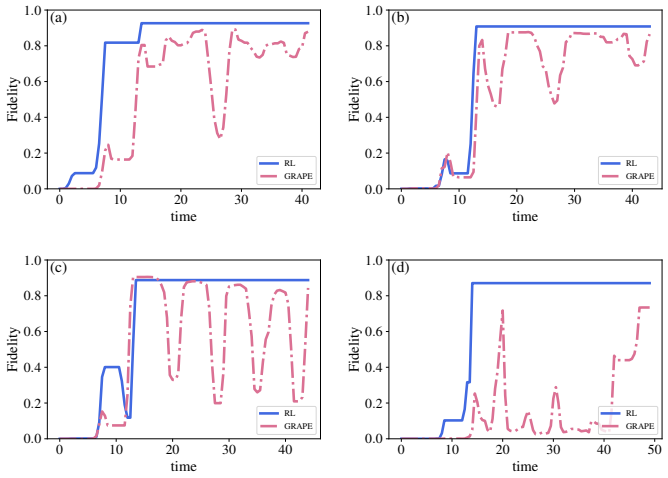


FIG. 8. Results from RL agent and GRAPE strategies for different high level control model with $\sqrt{\Gamma_d} = 0.1$.The horizontal and vertical axes of each subfigure denote evolution time t and fidelity $\mathcal{F}$. (A),(B),(C),(D): The evolution of fidelity with RL agent and GRAPE control of 4,6,8,10 level control model.

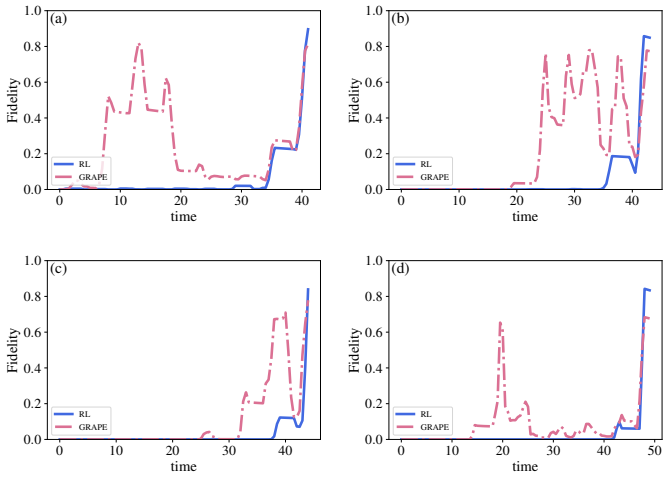


FIG. 9. Results from RL agent and GRAPE strategies for different high level control model with $\sqrt{\Gamma_l} = 0.1$. The horizontal and vertical axes of each subfigure denote evolution time t and fidelity $\mathcal{F}$. (A),(B),(C),(D): The evolution of fidelity with RL agent and GRAPE control of 4,6,8,10 level control model.

the control, because the energy of the system is decaying. The trajectory of GRAPE shows there indeed have many local minimas in the control landscape. However, the RL agent can with those those local minimas to find optimal strategies.

V. CONCLUSION

We propose a quantum control framework for multi-level dissipative quantum control optimization. The RL method is capable of finding the control protocol that has high-fidelity of a finite dimensional quantum control problem under disturbances and is superior to the traditional greedy method and GRAPE algorithm. Moreover, RL can accommodate switch on-off pulse shapes, which would be hard for traditional gradient methods.

Although the control problems dealt with the different dynamics optimization tasks, the RL agent can find high fidelity solutions with a single set of algorithmic hyperparameters. This suggests that learning the control landscape can be performed with minimal expert knowledge about the physical problem.

Our results, therefore, suggest that the RL based methods can be powerful alternatives to commonly used algorithms, capable of find control protocols that could be more efficient in practical complex quantum control problems. Also, the RL agent can be used to control experimental quantum devices. The present approach is flexible enough to be applied to different physical systems, such as qubit-cavity systems, weak measurements, and quantum error correction. We expect that our work would extend the deep learning techniques to deal with more practical quantum control problems in the near future.

ACKNOWLEDGMENTS

This work is supported by NSF of China (Grant Nos. 11775300 and 12075310), NKBRSF of China (Grant No. 2014CB921202), the National Key Research and Development Program of China (2016YFA0300603).

Appendix A: OPTIMAL LYAPUNOV QUANTUM CONTROL (GREEDY) METHOD

As the first trial, we consider a greedy way to get the optimal strategy. Greedy algorithms are used for finding successful policies because the algorithms are fast in converging on successful solutions when performing local searches. To describe the greedy method more intuitively, we use the optimal Lyapunov quantum control theory [1, 2, 62] to analyze the relationship between the strength of the control field and the control fidelity.

In Lyapunov quantum control, the control fields is determined by a Lyapunov function f, which will decrease with time. The evolution of the control protocol is determined by the Eq.(4). Further, we assume the system satisfy the requirement for a Lyapunov function, $f \geq 0$ [63]. The Lyapunov function can be defined as

$$f = \mathrm{Tr}(|n\rangle\langle n|\rho), \tag{A1}$$

The time derivative of the Lyapunov function is given by (with $[H_0, |n\rangle\langle n|] = 0$)

$$\begin{aligned} \dot{f} &= \mathrm{Tr}\left(|n\rangle\langle n|(-\frac{i}{\hbar}[H_0+V,\rho]+\mathcal{L}(\rho))\right) \\ &= \mathrm{Tr}(\mathcal{L}(\rho)|n\rangle\langle n|) - \frac{i}{\hbar}\mathrm{Tr}\left(\rho\left[|n\rangle\langle n|,\gamma(t)H_c\right]\right), \end{aligned} \tag{A2}$$

where $\mathcal{L}(\rho) = \sum_k \Gamma_k \left(A_k \rho A_k^\dagger - \frac{1}{2}\left\{A_k^\dagger A_k, \rho\right\}\right)$ and $H_c = \sum_{i=1}^{n-1}(|i\rangle\langle i+1| + |i\rangle\langle i+1|)$.It is clear that $\dot{f} \leq 0$, which ensures the decreasing of the Lyapunov function. So the control function $\gamma(t)$ satisfies:

$$\mathrm{Tr}(\mathcal{L}(\rho)|n\rangle\langle n|) \leq \gamma(t)\frac{i}{\hbar}\mathrm{Tr}\left(\rho\left[|n\rangle\langle n|, H_c\right]\right). \tag{A3}$$

Let

$$\begin{aligned} C &= \mathrm{Tr}(\mathcal{L}(\rho)|n\rangle\langle n|) \\ D &= \tfrac{i}{\hbar}\mathrm{Tr}\left(\rho\left[|n\rangle\langle n|, H_c\right]\right). \end{aligned} \tag{A4}$$

In our problem, the control function $\gamma(t)$ is always switches between two values, so the mathematical expressions of control fields as follows:

$$\gamma(t) = \begin{cases} \gamma & \text{if } D \geq 0, C > 0 \\ 0 & \text{if } D \geq 0, C \leq 0 \\ 0 & \text{if } D < 0, C > 0 \\ \gamma & \text{if } D < 0, C \leq 0 \end{cases}. \tag{A5}$$

Appendix B: Two-level case without dissipative

Consider a two-level system governed by the following Hamiltonian

$$H = -\frac{\omega}{2}\sigma_z + \gamma\sigma_x \tag{B1}$$

where we set$\hbar = 1$. $\omega$is the level spacing of the system,$\gamma = \gamma(t)$ denotes the control field. Assume that the aim is to steer the system from an arbitrary state$|\psi_0\rangle = \cos(\frac{\gamma_0}{2})|0\rangle + e^{i\phi}\sin(\frac{\gamma_0}{2})|1\rangle$ to state $|1\rangle$ (target state), where $|1\rangle$ is the excited state of the system, $|0\rangle$ is the excited state. Define a positive operator

$$P_e = \mathbf{I} - |0\rangle\langle 0| = |1\rangle\langle 1| \tag{B2}$$

The Lyapunov function can be written as

$$f_e = \mathrm{Tr}(P_e\rho) \tag{B3}$$

with

$$\rho = |\psi\rangle\langle\psi|, \quad |\psi\rangle = a(t)|0\rangle + b(t)|1\rangle \tag{B4}$$

The Lyapunov function f_e represents the overlapping between the function $\mathbf{I} - |0\rangle\langle 0|$ of target state $|1\rangle\langle 1|$ and the actual state of the system. The time derivative of

the Lyapunov function can be calculated as follows (with abbreviations, $a = a(t), b = b(t)$):

$$\begin{aligned}\dot{f}_e &= \mathrm{Tr}(P_e\rho) = \mathrm{Tr}(-iP_e[-\frac{\omega}{2}\sigma_z + \gamma\sigma_x, \rho]) \\ &= \mathrm{Tr}(-iP_e[-\frac{\omega}{2}\sigma_z, \rho]) + \mathrm{Tr}(-iP_e[\gamma\sigma_x, \rho]) \\ &= 2\gamma\mathrm{Im}(-ab^*)\end{aligned} \tag{B5}$$

If $f_e \leq 0$ for all times, f_e would monotonically decrease with time under the control, meanwhile the system is asymptotically steered into the target state $|1\rangle$. Using the method of greedy algorithm, the control field $\gamma(t)$ takes values

$$\gamma(t) = \begin{cases} \gamma & (\mathrm{Im}(-ab^*) < 0) \\ 0 & (\mathrm{Im}(-ab^*) \geq 0) \end{cases} \tag{B6}$$

With the optimal Lyapunov control, the time evolution of the two-level system can be analytically calculated. In a basis spanned by $\{|0\rangle, |1\rangle\}$, the total Hamiltonian can be expressed as

$$H = \sqrt{\frac{\omega^2}{4} + \gamma^2} \begin{pmatrix} -\cos(\theta) & \sin(\theta) \\ \sin(\theta) & \cos(\theta) \end{pmatrix} \tag{B7}$$

with θ defined by

$$\tan\theta = \frac{2f}{\omega}$$

The eigenvalues of the Hamiltonian H are

$$E_\pm = \pm\sqrt{\frac{\omega^2}{4} + \gamma^2} \tag{B8}$$

and the corresponding eigenvectors are given by,

$$|E_+\rangle = -\cos\frac{\theta}{2}|0\rangle + \sin\frac{\theta}{2}|1\rangle$$

$$|E_-\rangle = \sin\frac{\theta}{2}|0\rangle + \cos\frac{\theta}{2}|1\rangle$$

The time evolution operator can be calculated to be

$$U = exp(-iHt) = \begin{pmatrix} e^{-iE_-t}\cos^2\frac{\theta}{2} + e^{-iE_+t}\sin^2\frac{\theta}{2} & \frac{1}{2}(e^{-iE_+t} - e^{-iE_-t})\sin\theta \\ \frac{1}{2}(e^{-iE_+t} - e^{-iE_-t})\sin\theta & e^{-iE_-t}\sin^2\frac{\theta}{2} + e^{-iE_+t}\cos^2\frac{\theta}{2} \end{pmatrix} \tag{B9}$$

In the absence of a control field (i.e.,$\gamma(t) = 0$), we have $\theta = 0$. The time evolution operator reduces to a diagonal form,

$$U = \begin{pmatrix} e^{\frac{i\omega t}{2}} & 0 \\ 0 & e^{\frac{-i\omega t}{2}} \end{pmatrix}$$

Assume that the initial state of a two-level system is

$$|\psi_0\rangle = \cos(\frac{\gamma_0}{2})|0\rangle + e^{i\phi}\sin(\frac{\gamma_0}{2})|1\rangle = a_0|0\rangle + b_0|1\rangle$$

With different parameters $\gamma_0$and ψ, $|\psi_0\rangle$ can represent an arbitrary pure state. Let the target state $|1\rangle$ correspond to the south pole on the Bloch sphere. Since $\mathrm{Im}(-a_0b_0^*) = -\frac{\sin\phi\sin\gamma_0}{2}$, the first control field is calculated as,

$$\gamma(t) = \begin{cases} \gamma & (\mathrm{Im}(-ab^*) < 0), (0 < \theta < \pi) \\ 0 & (\mathrm{Im}(-ab^*) \geq 0), (\pi \leq \theta < 2\pi, \theta = 0) \end{cases} \tag{B10}$$

Assume that this control would last until time τ ; i.e., the duration of this control is τ . With this control, the state evolves to

$$\begin{aligned}|\psi_\tau\rangle =& [(e^{-iE_-t}\cos^2\frac{\theta}{2} + e^{-iE_+t}\sin^2\frac{\theta}{2})\cos\frac{\gamma_0}{2} + \frac{1}{2}(e^{-iE_+t} - e^{-iE_-t})\sin\theta e^{i\phi}\sin\frac{\gamma_0}{2}]|0\rangle \\ &+ [\frac{1}{2}(e^{-iE_+t} - e^{-iE_-t})\sin\theta\cos\frac{\gamma_0}{2} + (e^{-iE_-t}\sin^2\frac{\theta}{2} + e^{-iE_+t}\cos^2\frac{\theta}{2})e^{i\phi}\sin\frac{\gamma_0}{2}]|1\rangle \\ &\equiv a_\tau|0\rangle + b_\tau|1\rangle\end{aligned} \tag{B11}$$

From the design of the control law , we find that a control field would last until $\mathrm{Im}(-a_\tau b_t a u^*)$ changes sign. Then τ can be given by solving $\mathrm{Im}(-a_\tau b_t a u^*) = 0$: Meanwhile, the sign of $\mathrm{Im}(-a_\tau b_t a u^*)$ determines the next control field. Simple algebra shows that

$$\mathrm{Im}(-a_\tau b_\tau^*) = \frac{1}{2}(\sin(2E_-\tau)(\cos\theta\sin\gamma_0\cos\phi + \sin\theta\cos\gamma_0) + \sin\gamma_0\sin\phi\cos(2E_-\tau)) \tag{B12}$$

Appendix C: Distributed Proximal Policy Optimization

The Actor-Critic algorithm combines the advantages of policy-based and value-based methods. While the PPO algorithm [46, 47] based on Actor-Critic aims to optimize policy update. The central idea of Proximal Policy Optimization is to avoid having too large policy update which is proposed by trust region policy optimization (TRPO) [64]. The underlying idea of such improvements thereby is limiting the magnitude of updates to θ by imposing constraints on the difference between $\pi_{\theta\ \mathrm{old}}$ and π_θ in order to prevent catastrophic jumps out of optima and achieve a better convergence behavior.

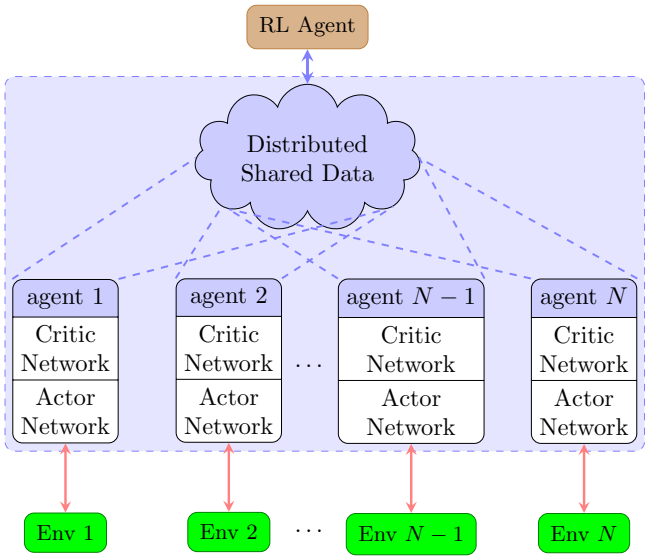


FIG. 10. Schematics of the DPPO algorithm. Data collection and gradient calculation are distributed over workers, labeled as "agent i". Then the weights of RL agent update synchronously. The environments, labeled as "env i".

One main novelty hereby lies in the introduced loss of DPPO,

$$\begin{aligned} L^{CLIP}(\theta) =& \mathbb{E}_t\left[\min\left(r_t(\theta)A_t(s,a)\ ,\right.\right. \\ & \left.\left.\mathrm{clip}\left(r_t(\theta), 1-\epsilon, 1+\epsilon\right)A_t(s,a)\right)\right] \end{aligned} \tag{C1}$$

where $\mathbb{E}_t$ and $A_t(s,a)$ are the expectation over time steps and the advantage at time t respectively. If $r_t(\theta) > 1$, the action is more probable in the current policy than the old policy; if $r_t(\theta) > 1$ is between 0 and 1, the action is less probable for current policy than for the old one.

As consequence, a new objective function from Eq.(11) could be

$$L^{CPI}(\theta) = \hat{\mathbb{E}}_t\left[\frac{\pi_\theta(a|s)}{\pi_{\theta\ \mathrm{old}}(a|s)}A_t(s,a)\right] = \hat{\mathbb{E}}_t\left[r_t(\theta)A_t(s,a)\right]. \tag{C2}$$

However, without a constraint, if the action taken is much more probable in our current policy than in our former, this would lead to a large policy gradient step and consequence an excessive policy update.

So the PPO algorithm clip probability ratio directly in the objective function with its Clipped surrogate objective function[Eq. C1]. The loss function poses a lower bound on the improvement induced by an update and hence establishes a trust region around $\pi_{\theta\ \mathrm{old}}$. The hyperparameter θ controls the maximal improvement and thus the size of the trust region.

Algorithm 1: Distributed Proximal Policy Optimization

```
Randomly initialize critic network V_φ(s) and actor
  π_θ(a|s) with weights φ and θ;
for iteration ∈ {1, 2, ..., C} do
    for actor = 0, ..., N do
        Initialize s_0;
        Run policy π_θ (T/δt) times, collecting
          {s_t, a_t, R_{t+1}};
        Estimate advantages
          A_t = Σ_{t'>t} γ^{t'-t} R_{t'} − V_φ(s_t);
        Estimate V̂_t = A_t + V_φ(s_t);
    end
    π_{θ_old} ← π_θ
    for j ∈ {1, ..., M} do
        J_PPO(θ) =
          [min(r_t(θ)A_t , clip(r_t(θ), 1−ε, 1+ε) A_t)];
        Update θ by a gradient method w.r.t. J_PPO;
          J_critic(φ) = −E_t (V̂_t − V_φ(s_t))^2;
        Update φ by a gradient method w.r.t.
          J_critic(φ)
    end
end
```

In order to improve the efficiency of the learning process, a distributed version of PPO algorithm (DPPO) [46], is implemented in our calculation[Fig. 10].Algorithm 1 shows the pseudocode for the DPPO.

Appendix D: The effect of distribution of eigenenergies

In the main text we use a regular distribution of eigeneneriges to test our algorithm. However, a different distribution of eigenenergy would affect the perfor-

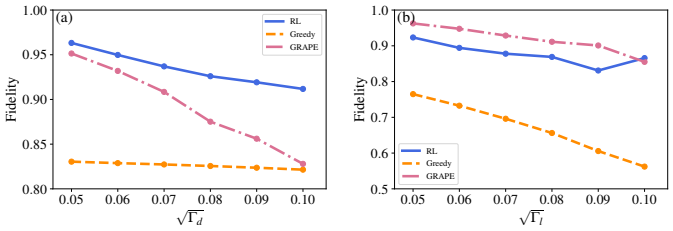


FIG. 11. Results from the three algorithms for 4 level control model with the Hamiltonian of (i) under disturbances. The horizontal and vertical axes of each subfigure denote noise rate $\sqrt{\Gamma_{k,n}}$ and fidelity $\mathcal{F}$. (A): dephasing dynamics (B): energy decay dynamics.

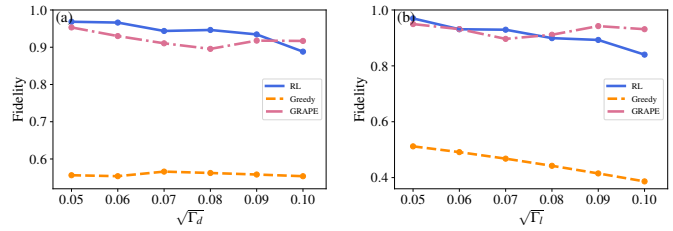


FIG. 12. Results from the three algorithms for 4 level control model with the Hamiltonian of (ii) under disturbances. The horizontal and vertical axes of each subfigure denote noise rate $\sqrt{\Gamma_{k,n}}$ and fidelity $\mathcal{F}$. (A): dephasing dynamics (B): energy decay dynamics.

mance of the algorithm. The effect of distribution of eigenenergies was examined for two example cases, (i) the eigenenergy E_i extracted from the uniform distribution with $E_1 = 0.40252154, E_2 = 0.68846289, E_3 = 0.8557115, E_4 = 0.25471114$ and (ii) the eigenenergy E_i has degenerate in the middle with $E_1 = 1, E_2 = E_3 = 2, E_4 = 3$.

As Fig. 11 and Fig. 12 shown, the performance of the three algorithms is affected under the different energy distribution. However, the GRAPE algorithm and our algorithm still maintain superiority over the greedy algorithm. This is consistent with what we discussed in the main text.

Appendix E: Hyper-Parameters and Learning Curves

Our RL agent makes use of two deep neural networks to approximate the values for the possible actions of each state and the optimal policy. Each network consists of 4 layers. All layers have ReLU activation functions except the output layer which has linear activation. The hyper-parameters of the network are summarized in Table I.

All algorithms are implemented with Python 3.6, and have been run on two 14-core 2.60GHz CPU with 188 GB memory and four GPUs.

TABLE I. Training Hyper-Parameters

Hyper-parameter	Values
Neurons in actor network	$\{1024, 1024, 1024, 1024\}$
Neurons in critic network	$\{1024, 1024, 1024, 1024\}$
Actor numbers N	12
Batch size	[a]
PPO clipping ϵ	0.2
Learning rate	0.0001[b]
Update steps M	15
Reward decay Γ	0.85
Total episode C	[c]

[a] is the same as the time steps
[b] With Adam algorithm
[c] different for various tasks

[1] P. Vettori, in *Proceedings of the MTNS Conference* (2002) pp. 1–6.
[2] S. Grivopoulos and B. Bamieh, in *42nd IEEE International Conference on Decision and Control (IEEE Cat. No. 03CH37475)*, Vol. 1 (IEEE, 2003) pp. 434–438.
[3] V. Jurdjevic, *Geometric Control Theory*, Cambridge Studies in Advanced Mathematics (Cambridge University Press, 1996).
[4] D. V. Zhdanov and T. Seideman, arXiv preprint arXiv:1709.09423 (2017).
[5] C. Avinadav, R. Fischer, P. London, and D. Gershoni, Physical Review B **89**, 245311 (2014).
[6] K. Xia, J. Twamley, *et al.*, Phys. Rev. X **3**, 031013 (2013).
[7] J. Plantenberg, P. De Groot, C. Harmans, and J. Mooij, Nature **447**, 836 (2007).
[8] N. Khaneja, T. Reiss, C. Kehlet, T. Schulte-Herbrüggen, and S. J. Glaser, Journal of Magnetic Resonance **172**, 296 (2005).
[9] T. Schulte-Herbrüggen, A. Spörl, N. Khaneja, and S. J. Glaser, Phys. Rev. A **72**, 042331 (2005).
[10] P. Doria, T. Calarco, and S. Montangero, Phys. Rev. Lett. **106**, 190501 (2011).
[11] T. Caneva, T. Calarco, and S. Montangero, Phys. Rev. A **84**, 022326 (2011).
[12] M. A. Nielsen and I. L. Chuang, *Quantum Computation and Quantum Information* (Cambridge University Press, 2010).
[13] P. W. Shor, Phys. Rev. A **52**, R2493 (1995).
[14] A. M. Steane, Phys. Rev. Lett. **77**, 793 (1996).
[15] E. Knill and R. Laflamme, Phys. Rev. A **55**, 900 (1997).
[16] P. Zanardi and M. Rasetti, Phys. Rev. Lett. **79**, 3306 (1997).
[17] L. Viola, E. Knill, and S. Lloyd, Phys. Rev. Lett. **82**, 2417 (1999).
[18] W. Yang and R.-B. Liu, Phys. Rev. Lett. **101**, 180403 (2008).

[19] X. Xu, Z. Wang, C. Duan, P. Huang, P. Wang, Y. Wang, N. Xu, X. Kong, F. Shi, X. Rong, and J. Du, Phys. Rev. Lett. **109**, 070502 (2012).
[20] G. S. Uhrig, Phys. Rev. Lett. **98**, 100504 (2007).
[21] A. G. Kofman and G. Kurizki, Phys. Rev. Lett. **87**, 270405 (2001).
[22] P. Palittapongarnpim, P. Wittek, E. Zahedinejad, S. Vedaie, and B. C. Sanders, Neurocomputing **268**, 116 (2017).
[23] M. Born and V. Fock, Zeitschrift für Physik **51**, 165 (1928).
[24] O. Astafiev, Y. A. Pashkin, Y. Nakamura, T. Yamamoto, and J. S. Tsai, Phys. Rev. Lett. **93**, 267007 (2004).
[25] A. Shimizu and M. Ueda, Phys. Rev. Lett. **69**, 1403 (1992).
[26] M. R. Delbecq, T. Nakajima, P. Stano, T. Otsuka, S. Amaha, J. Yoneda, K. Takeda, G. Allison, A. Ludwig, A. D. Wieck, and S. Tarucha, Phys. Rev. Lett. **116**, 046802 (2016).
[27] C. H. Henry and R. F. Kazarinov, Rev. Mod. Phys. **68**, 801 (1996).
[28] F. Petruccione and H.-P. Breuer, *The theory of open quantum systems* (Oxford Univ. Press, Berlin, 2002).
[29] K. Børkje, A. Nunnenkamp, J. D. Teufel, and S. M. Girvin, Phys. Rev. Lett. **111**, 053603 (2013).
[30] C. Avinadav, R. Fischer, P. London, and D. Gershoni, Phys. Rev. B **89**, 245311 (2014).
[31] U. Boscain, Journal of Mathematical Physics **43**, 2107 (2002).
[32] M. Hirose and P. Cappellaro, Quantum Information Processing **17**, 88 (2018).
[33] M. Bukov, A. G. R. Day, D. Sels, P. Weinberg, A. Polkovnikov, and P. Mehta, Phys. Rev. X **8**, 031086 (2018).
[34] T. Caneva, T. Calarco, R. Fazio, G. E. Santoro, and S. Montangero, Phys. Rev. A **84**, 012312 (2011).
[35] D. Silver, A. Huang, C. J. Maddison, A. Guez, L. Sifre, G. van den Driessche, J. Schrittwieser, I. Antonoglou, V. Panneershelvam, M. Lanctot, S. Dieleman, D. Grewe, J. Nham, N. Kalchbrenner, I. Sutskever, T. Lillicrap, M. Leach, K. Kavukcuoglu, T. Graepel, and D. Hassabis, Nature **529**, 484 (2016).
[36] D. Silver, J. Schrittwieser, K. Simonyan, I. Antonoglou, A. Huang, A. Guez, T. Hubert, L. Baker, M. Lai, A. Bolton, *et al.*, Nature **550**, 354 (2017).
[37] D. Silver, T. Hubert, J. Schrittwieser, I. Antonoglou, M. Lai, A. Guez, M. Lanctot, L. Sifre, D. Kumaran, T. Graepel, T. Lillicrap, K. Simonyan, and D. Hassabis, Science **362**, 1140 (2018).
[38] V. Mnih, K. Kavukcuoglu, D. Silver, *et al.*, Nature **518**, 529 (2015).
[39] O. Vinyals, I. Babuschkin, W. M. Czarnecki, M. Mathieu, A. Dudzik, J. Chung, D. H. Choi, R. Powell, T. Ewalds, P. Georgiev, J. Oh, D. Horgan, M. Kroiss, I. Danihelka, A. Huang, L. Sifre, T. Cai, J. P. Agapiou, M. Jaderberg, A. S. Vezhnevets, R. Leblond, T. Pohlen, V. Dalibard, D. Budden, Y. Sulsky, J. Molloy, T. L. Paine, C. Gulcehre, Z. Wang, T. Pfaff, Y. Wu, R. Ring, D. Yogatama, D. Wünsch, K. McKinney, O. Smith, T. Schaul, T. Lillicrap, K. Kavukcuoglu, D. Hassabis, C. Apps, and D. Silver, Nature **575**, 350 (2019).
[40] M. Jaderberg, W. M. Czarnecki, I. Dunning, L. Marris, G. Lever, A. G. Castañeda, C. Beattie, N. C. Rabinowitz, A. S. Morcos, A. Ruderman, N. Sonnerat, T. Green, L. Deason, J. Z. Leibo, D. Silver, D. Hassabis, K. Kavukcuoglu, and T. Graepel, Science **364**, 859 (2019).
[41] H. Yu, X. Xu, H. Ma, Z. Zhu, and C. Chen, in *2018 33rd Youth Academic Annual Conference of Chinese Association of Automation (YAC)* (IEEE, 2018) pp. 922–927.
[42] Z. An and D. L. Zhou, EPL **126**, 60002 (2019).
[43] M. Y. Niu, S. Boixo, V. N. Smelyanskiy, and H. Neven, npj Quantum Information **5**, 33 (2019).
[44] T. Fösel, P. Tighineanu, T. Weiss, and F. Marquardt, Phys. Rev. X **8**, 031084 (2018).
[45] H. Xu, J. Li, L. Liu, Y. Wang, H. Yuan, and X. Wang, npj Quantum Information **5**, 82 (2019).
[46] N. Heess, S. Sriram, J. Lemmon, J. Merel, G. Wayne, Y. Tassa, T. Erez, Z. Wang, S. Eslami, M. Riedmiller, *et al.*, arXiv preprint arXiv:1707.02286 (2017).
[47] J. Schulman, F. Wolski, P. Dhariwal, A. Radford, and O. Klimov, arXiv preprint arXiv:1707.06347 (2017).
[48] J. C. V. Tieck, M. V. Pogančić, J. Kaiser, A. Roennau, M.-O. Gewaltig, and R. Dillmann, in *Artificial Neural Networks and Machine Learning – ICANN 2018*, edited by V. Kůrková, Y. Manolopoulos, B. Hammer, L. Iliadis, and I. Maglogiannis (Springer International Publishing, Cham, 2018) pp. 211–221.
[49] E. Bøhn, E. M. Coates, S. Moe, and T. A. Johansen, in *2019 International Conference on Unmanned Aircraft Systems (ICUAS)* (2019) pp. 523–533.
[50] M. August, J. M. Hernández-Lobato, M. August, and J. M. Hernández-Lobato, *International Conference on High Performance Computing*, , 591 (2018).
[51] J.-J. Chen and M. Xue, Manipulation of spin dynamics by deep reinforcement learning agent (2019), arXiv:1901.08748 [quant-ph].
[52] C. Watkins, *Learning From Delayed Rewards*, Ph.D. thesis, Cambridge University Psychology Department (1989).
[53] R. S. Sutton and A. G. Barto, *Reinforcement Learning: An Introduction* (MIT Press, 1998).
[54] J. Schulman, P. Moritz, S. Levine, M. I. Jordan, and P. Abbeel, in *4th International Conference on Learning Representations, ICLR 2016, San Juan, Puerto Rico, May 2-4, 2016, Conference Track Proceedings*, edited by Y. Bengio and Y. LeCun (2016).
[55] A. Shapiro, Handbooks in operations research and management science **10**, 353 (2003).
[56] V. Mnih, A. P. Badia, M. Mirza, A. Graves, T. Lillicrap, T. Harley, D. Silver, and K. Kavukcuoglu, in *International conference on machine learning* (2016) pp. 1928–1937.
[57] G. Brockman, V. Cheung, L. Pettersson, J. Schneider, J. Schulman, J. Tang, and W. Zaremba, Openai gym (2016), arXiv:1606.01540.
[58] M. Abadi, A. Agarwal, P. Barham, E. Brevdo, Z. Chen, C. Citro, G. S. Corrado, A. Davis, J. Dean, M. Devin, S. Ghemawat, I. Goodfellow, A. Harp, G. Irving, M. Isard, Y. Jia, R. Jozefowicz, L. Kaiser, M. Kudlur, J. Levenberg, D. Mané, R. Monga, S. Moore, D. Murray, C. Olah, M. Schuster, J. Shlens, B. Steiner, I. Sutskever, K. Talwar, P. Tucker, V. Vanhoucke, V. Vasudevan, F. Viégas, O. Vinyals, P. Warden, M. Wattenberg, M. Wicke, Y. Yu, and X. Zheng, TensorFlow: Large-scale machine learning on heterogeneous systems (2015), software available from tensorflow.org.
[59] P. Dhariwal, C. Hesse, O. Klimov, A. Nichol, M. Plap-

pert, A. Radford, J. Schulman, S. Sidor, Y. Wu, and P. Zhokhov, Openai baselines, https://github.com/openai/baselines (2017).

[60] J. Johansson, P. Nation, and F. Nori, Computer Physics Communications **183**, 1760 (2012).

[61] J. Johansson, P. Nation, and F. Nori, Computer Physics Communications **184**, 1234 (2013).

[62] L. Wang, S. Hou, X. Yi, D. Dong, and I. R. Petersen, Physics Letters A **378**, 1074 (2014).

[63] D. d'Alessandro, *Introduction to quantum control and dynamics* (Chapman and Hall/CRC, 2007).

[64] J. Schulman, S. Levine, P. Moritz, M. I. Jordan, and P. Abbeel, Trust region policy optimization (2015), arXiv:1502.05477 [cs.LG].